Received: 6 December 2022 | Revised: 7 March 2023 | Accepted: 7 March 2023

DOI: 10.1002/pol.20220721

RESEARCH ARTICLE

JOURNAL OF POLYMER SCIENCE WILEY

Dynamic monomers for Hot Lithography: The UPy motif as a versatile tool towards stress relaxation, reprocessability, and 3D printing

Larissa Alena Ruppitsch[1] | **Jakob Ecker**[2] | **Thomas Koch**[2] | **Katharina Ehrmann**[1] | **Jürgen Stampfl**[2] | **Robert Liska**[1]

[1]Institute of Applied Synthetic Chemistry, Technische Universität Wien, Vienna, Austria

[2]Institute of Materials Science and Technology, Technische Universität Wien, Vienna, Austria

Correspondence
Robert Liska, Institute of Applied Synthetic Chemistry, Technische Universität Wien, Getreidemarkt 9/163 MC, 1060 Vienna, Austria.
Email: robert.liska@tuwien.ac.at

Abstract

Supramolecular polymers can substantially influence the dynamic mechanical properties in slightly crosslinked polymer networks. One prominent example of supramolecular building blocks is 2-ureido-4[1H]-pyrimidinones (UPy). Combining UPy-terminated supramolecular segments with classical covalent-reactive monomers implements dynamic behavior in photopolymerizable systems. In this work, a UPy-based methacrylic monomer (up to 20 mol%) was introduced in a classical photopolymerizable methacrylate matrix. The influence of the UPy-motif on the reactivity and (thermo)mechanical properties was investigated via RT-NIR photorheology, DMTA, and tensile testing. The dynamic behavior was characterized via stress relaxation and reprocessing studies to demonstrate the dynamic effects of photopolymers containing the UPy building block compared to difunctional photopolymers with similar structural features. In a final step, the UPy-based photopolymerizable system was applied in bulk in a Hot Lithography printing process at elevated temperatures yielding complex 3D-printed parts with high resolution and precision.

KEYWORDS

3D-printing, bulk, dynamic monomers, Hot Lithography, quadruple hydrogen bonding, reprocessability, reversibility, stress relaxation

1 | INTRODUCTION

Supramolecular polymers (SMPs) were established more than 25 years ago, in pioneering work of Stupp et al.[1] and Meijer et al.[2] exploring their structures and physical properties.[3] SMPs can be classified as aggregates of low molecular weight molecules connected via strong non-covalent interactions to obtain a polymer with a collective molecular weight.[4] The dynamic equilibrium between the bonded and open form of such non-covalent interactions generates adaptable SMP-properties, which can be triggered by external stimuli such as light, temperature, or water due to their ability to influence the bonding equilibrium.[5–8]

These dynamic properties manifest themselves in several effects like self-healing,[9,10] shape-memory[11-13] and (de)bonding on demand[14] and they can also be exploited in

a range of applications such as simplified processing,[15,16] reprocessing[17] and recycling.[18-20] Unfortunately, SMPs usually show mechanical properties similar to elastomers and plastics,[4] whereas a thermoset-like behavior is required for several applications. Therefore, research focused on so-called hybrid bonding polymers, where covalent and non-covalent reacting sites were combined in one monomer to reconcile the dynamic character with mechanical strength.[21,22] The difference in the mechanical behavior compared to pure SMPs can be explained by the covalent attachment of the H-bonding unit, which weakens the influence of the supramolecular structure.[23] Hybrid bonding monomers have been shown to copolymerize efficiently and therefore give rise to a vast field of applications (e.g., 3D-printing,[24] coatings and adhesives,[25] regenerative medicine,[3] thermal and light-responsive actuation in soft robotics[26]).

Many different approaches are presented in literature[4] to obtain these non-covalent interactions in the macromolecule like metal–ligand interactions,[27,28] π − π stacking,[29] or hydrogen bonding motifs.[2] In general, hydrogen bonding is a relatively weak non-covalent interaction exhibiting bonding energies around 10 times smaller than classical C-C bonds.[30] Single, double, and triple hydrogen bonds exhibit insufficient stability resulting in minor research for dynamic bonding applications.[2] However, the development of the quadruple hydrogen bonding motif 2-ureido-4 [1H]-pyrimidinones (UPy) by Meijer and co-workers[2] triggered enormous interest due to the strong dimerization and higher bond energy of UPy compared to other H-bonding systems (Figure 1).[31,32]

This strong dimerization can be observed in two tautomeric forms (Figure 1) and is thermoreversible at temperatures around 80°C. This originates from the equilibrium between the open form at higher temperatures with dissociated H-bonds and the closed form at lower temperatures, where these H-bonds are present. Therefore, the choice of processing temperature influences not only the processability demonstrated by lower viscosities but also the thermal stability, solubility, and material properties of the final polymer.[33,34] The main issue of hybrid bonding polymers using the UPy-motif as a non-covalent bonding site is its limited solubility in bulk and in solvents.[31,35,36] Pioneering work was performed by Heinzmann et al.,[37] who developed the first liquid hybrid-bonding monomer based on a UPy-unit connected via an amine-terminated oligo(propylene glycol) to a methacrylic end group (Figure 2). The liquid state of this monomer originates from introducing the relatively long ether-based spacer, which lowers the dimerization constant via competitive binding with the UPy-unit. Additionally, this monomer shows excellent miscibility with commercially available methacrylates (e.g., BnMA, BMA, HMA, HEMA) and relatively good reactivities during free-radical bulk copolymerization. Furthermore, it was demonstrated that up to 20 mol% of this hybrid bonding monomer copolymerized with several methacrylates exhibit the best hydrogen-bonding ability.[37]

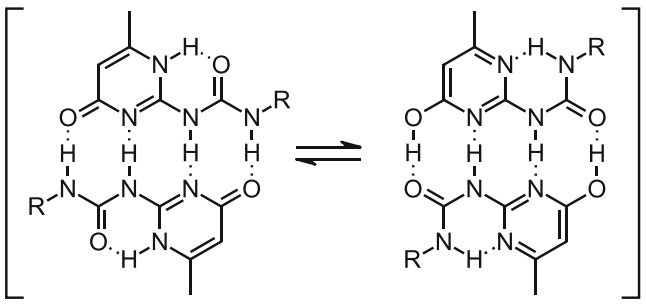

FIGURE 1 Chemical structure of quadruple hydrogen bonding of the UPy-unit with hydrogen-bonding interactions displayed by dotted lines.

The UPy motif already found application in several additive manufacturing processes (e.g., fused filament fabrication,[24] direct ink writing,[38] digital light projection[39]), opening new possibilities for future developments in the sector of 3D-printing. Unfortunately, most UPy-based monomers are solids exhibiting melting points above 100°C due to the strong dimerization of the H-bonds, which aggravates the printing process. Recent research tried to overcome this issue by printing a solid UPy-based monomer in solution at elevated temperature, but at the expense of resolution.[39] A different approach would be to use the lithography-based additive manufacturing technology Hot Lithography,[40] which can process highly viscous resins in bulk (up to 20 Pa · s) at elevated temperatures (50–120°C) with high feature resolution and precision.

Therefore, the liquid monomer UPy (Figure 2) was chosen to investigate its dynamic influence on the final polymer network and its usability in a Hot Lithography process in bulk. We present the comparison of UPy with a covalently bonding difunctional reference compound (REF) in a methacrylic matrix (MAM) and with the pure matrix system MAM. The reactivity of all three systems (UPy, REF, and MAM) is analyzed via RT-NIR photorheology studies, followed by the investigation of the (thermo)mechanical properties employing DMTA and tensile testing to determine the influence of the UPy monomer in MAM as opposed to the covalently bonded difunctional monomer REF. The dynamic behavior is characterized via stress relaxation and reprocessability studies to highlight the benefits of UPy. Afterwards, thermal stability, storage stability, and viscosity of the monomers are investigated to evaluate the usability in a 3D-printing process at elevated temperatures. Finally, a complex 3D structure is printed from the UPy-containing

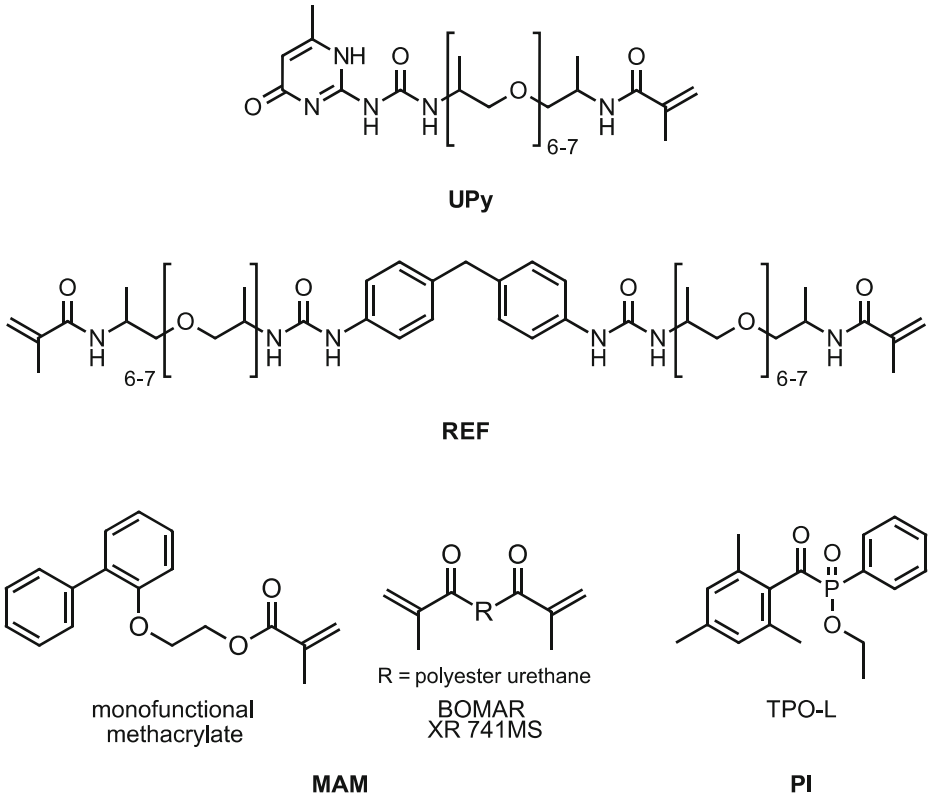

FIGURE 2 Chemical structures of the compounds UPy, REF, MAM (monofunctional methacrylate and difunctional crosslinker BOMAR XR 741 MS), and the photoinitiator TPO-L.

formulation in bulk via Hot Lithography and investigated under a scanning electron microscope to highlight the high resolution and precision of the printed part.

2 | RESULTS AND DISCUSSION

2.1 | Synthesis of UPy and REF-monomers and design of matrix formulation

The synthesis of UPy was conducted in a three-step procedure from Wong et al.[41] and Heinzmann et al. (Figures 2 and 3).[37] The first step was the activation of the UPy-building block 2-amino-4-hydroxy-6-methylpyrimidine with 1,1′-carbonyl-diimidazole, which yielded 93% product. In the second step, the activated UPy-unit was coupled with an amine-terminated oligo(propylene glycol) and purified with column chromatography to obtain 74% of the intermediate product. In the third step, this intermediate was methacrylated with methacrylic anhydride to provide covalent reactivity and afterwards purified via column chromatography to yield 46% of the desired monomer UPy. The UPy-unit shows a strong dimerization of the quadruple H-bonds below 80°C. In this prevalently dimerized state, the hybrid bonding compound UPy exhibits two photopolymerizable groups, mimicking a difunctional methacrylate at room temperature. Consequently, a difunctional reference compound REF (Figures 2 and 4) was envisioned. The synthesis of this compound was analogue to the three-step synthesis of the UPy monomer, using the difunctional starting material 4,4′-methylenedianiline (MDA).

As methacrylic matrix (MAM), a monofunctional methacrylic monomer was targeted. Previous studies by Catel et al.[42] highlight the good properties of the monofunctional methacrylic monomer 2-(2-phenylphenoxy) ethyl methacrylate (Figure 2), suggesting its use as main component in MAM. Since hydrogen bonding is reversible at temperatures above 80°C, a difunctional crosslinker based on polyester urethane methacrylates (BOMAR XR 741 MS) was added to improve the material properties of this monofunctional methacrylate. Several examples in literature already proved that slight crosslinks do not interfere with the dynamic hydrogen bonding properties.[39,43] TPO-L was chosen as photoinitiator due to its good miscibility with methacrylic monomers. Both monomers (UPy and REF) were added to MAM in concentrations up to 20 mol% (Table S1). All three systems (UPy, REF, and MAM) were characterized regarding their reactivity, (thermo)mechanical, and dynamic properties, as well as their use in a Hot Lithography printing process.

The reactivity of the monomers UPy and REF in MAM and the (thermo)mechanical behavior of the corresponding polymers were studied with RT-NIR photorheology, DMTA, and tensile testing. Both studies were

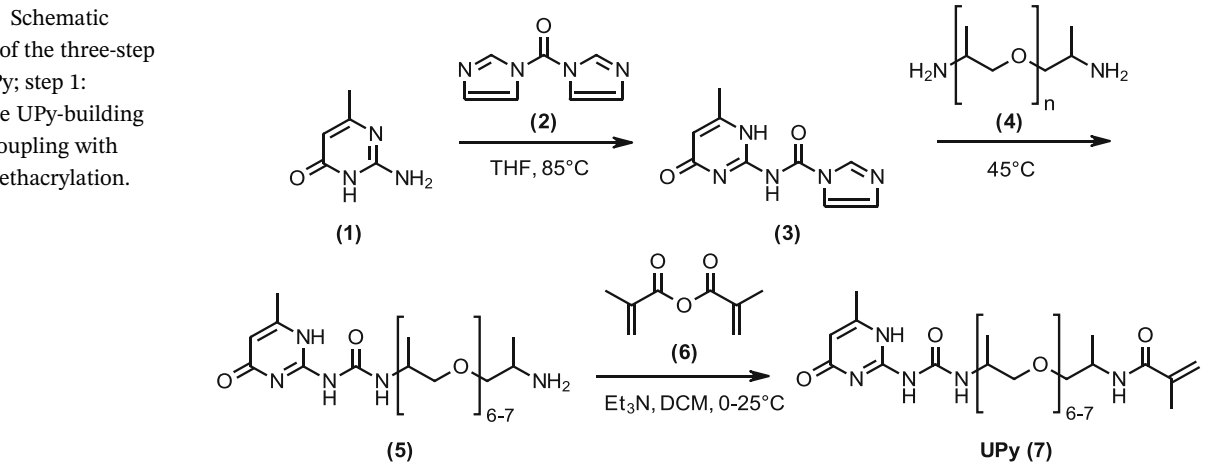

FIGURE 3 Schematic representation of the three-step synthesis of UPy; step 1: activation of the UPy-building block, step 2: coupling with OPG, step 3: methacrylation.

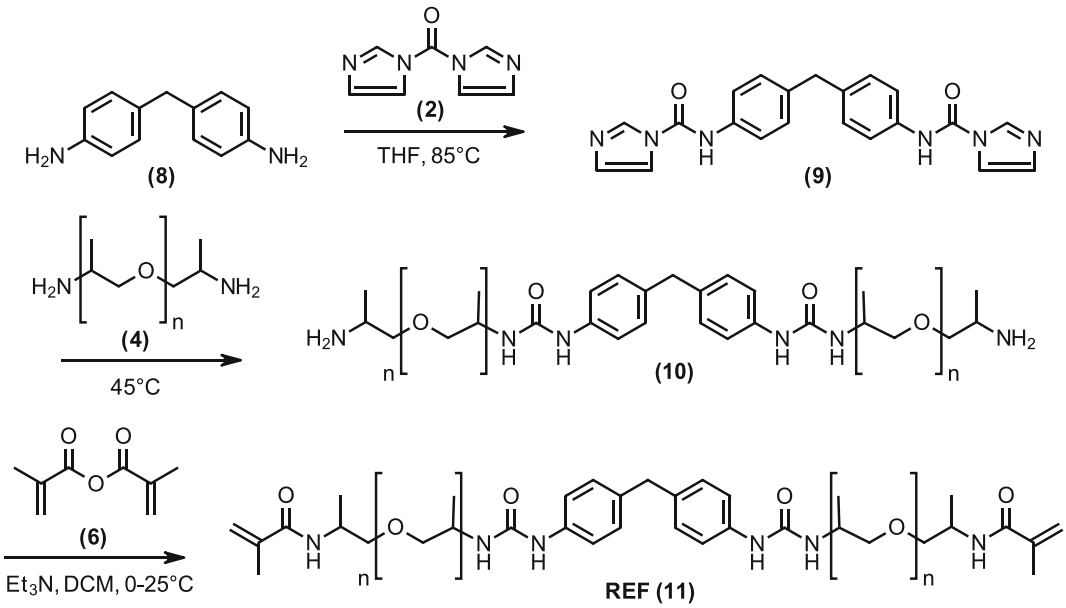

FIGURE 4 Schematic representation of the three-step synthesis of REF; step 1: activation of the MDA-building block, step 2: coupling with OPG, step 3: methacrylation.

performed using different concentrations of the monomers UPy and REF in MAM (0 mol%, 5 mol%, 10 mol%, 15 mol%, and 20 mol%) to analyze the impact of increasing monomer content (Figures S1-S2, Tables S2-S4). The resulting formulations are therefore described by the type of monomer added to MAM (i.e. UPy or REF) and by the amount of added monomer (i.e. 0 mol %, 5 mol%, ..., 20 mol%). For example, "UPy-20%" describes a formulation containing 20 mol% UPy and 80 mol% MAM. All investigations of the dynamic properties and 3D printing were only performed with 20 mol% of UPy and REF, as well as the pure MAM to demonstrate the impact of the dynamic bonds in the best way.

2.2 | Reactivity and polymerization study

2.2.1 | RT-NIR photorheology

The photoinduced polymerization process and chemical conversion can be evaluated simultaneously via RT-NIR photorheology measurements.[44] The influence of adding up to 20 mol% UPy to MAM in comparison to the difunctional REF and pure MAM on the reaction speed, chemical conversion, and volumetric shrinkage was investigated. Since methacrylic monomers usually are highly reactive and exhibit fast gelation, the gel point (t_{gel}), which is the intersection of storage (G') and loss modulus (G''), is reached at

an early stage. At this point, a high double bond conversion (DBC_{gel}) is targeted to allow for high overall conversion and avoid build-up of shrinkage stress because the chain mobility is restricted after gelation. The two key characteristics of this analysis method are the final double bond conversion (DBC_{final}) and shrinkage behavior. The DBC_{final} values can be calculated by comparing the integrated NIR-signals at a wavelength of around 6100–6300 cm^{-1} over the polymerization process. Shrinkage behavior can be determined via the normal force (F_N). Since the shrinkage force increases with increasing conversion, the comparison must be drawn at an equal conversion value ($F_{N\ DBC\ 80\%}$). However, the flexibility of a material determined via the final storage modulus (G') needs to be taken into consideration since this effect also influences shrinkages behavior.

Figure 5 depicts the conversion and shrinkage behavior of MAM, UPy-20%, and REF-20% at 25 and 50°C. The final conversion of all formulations is generally high (DBC > 88%, Figure 5A, Table 1). The addition of the UPy-monomer increases conversion compared to MAM, while the REF compound does not influence the conversion significantly, which is surprising since difunctional monomers usually exhibit lower conversion rates. As expected, the conversion further improves at 50°C for all formulations and higher conversions are still achieved with increasing amount of UPy (Figure S1, Table S2-3). The slope at the beginning of the curve represents the reaction speed of polymerization (R_p, Figure 5B, Table 1). Herein, it is visible that REF-20% has the lowest R_p at 25 and 50°C (R_p > 12% s^{-1}), while MAM and UPy-20% show a significantly increased R_p (R_p > 20% s^{-1}).

The addition of both UPy and REF shifts t_{gel} at 25°C to later stages compared to MAM (t_{gel}: UPy-20% = 2.5 s, REF-20% = 2.4 s, MAM = 2.0 s, Figure 5B, Table 1, Table S2-3) but at 50°C UPy-20% exhibits an earlier t_{gel} compared to MAM (t_{gel}: UPy-20% = 1.4 s, MAM = 1.9 s). This can be explained by the partial dissociation of the H-bonds at 50°C allowing higher mobility in the formulation and consequently increasing the overall reactivity. At both temperatures, DBC_{gel} of UPy-20% and MAM is in the same range, while the REF-20%-compound shows lower values indicating reduced chain mobility during the polymerization process despite the later t_{gel}.

The shrinkage behavior at an equal conversion level of 80% ($F_{N\ DBC\ 80\%}$) further highlights the positive impact of the UPy-compound on the network by demonstrating its reduced shrinkage compared to MAM (Figure 6, Table 1, Table S2). The REF-20% compound reduces shrinkage even more than UPy-20%. This result is caused by the flexible long spacer unit of the REF-compound causing a more flexible final polymer. The storage modulus (G') further underlines this result showing G'-values for MAM and

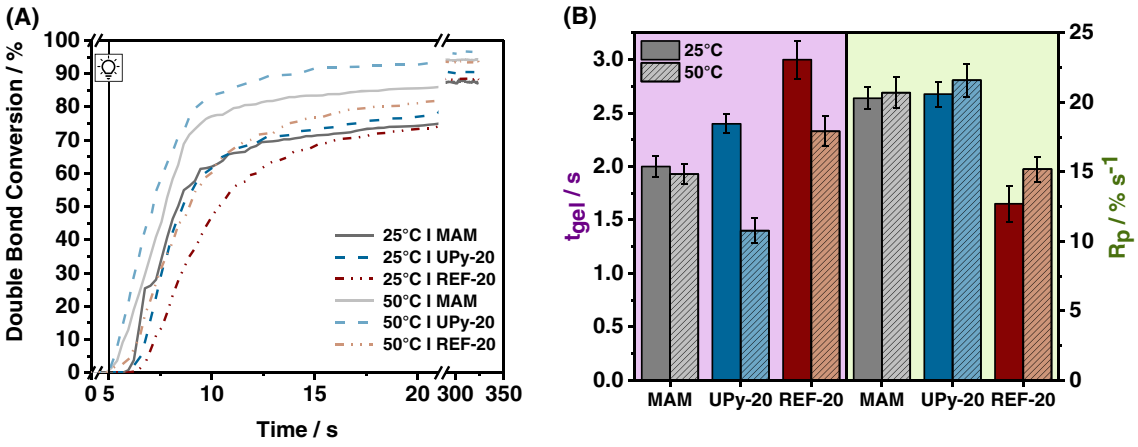

FIGURE 5 RT-NIR photorheology at 25°C and 50°C, (A): double bond conversion (DBC); (B): gelation point (t_{gel}) and reaction speed of polymerization (R_p) of MAM, UPy-20%, and REF-20%; irradiation started after 5 s (black line in (A)).

TABLE 1 Gel point (t_{gel}), double bond conversions (DBC_{gel}, DBC_{95}, DBC_{final}), storage modulus (G'), reaction speed of polymerization (R_p) and shrinkage behavior (F_N final, $F_{N\ DBC\ 80\%}$) at 25 and 50°C.

	25°C							50°C			
	t_{gel}/s	DBC_{gel}/%	DBC_{final} /%	R_P/% s^{-1}	G'/MPa	$F_N$final/N	$F_{N\ DBC\ 80\%}$/N	t_{gel} /s	DBC_{gel} /%	DBC_{final}/%	R_P/% s^{-1}
MAM	2	38.7	88.3	20.3	516	−20.0	−17.6	1.93	35.0	94.2	20.7
UPy-20%	2.4	39.8	92.7	20.6	454	−17.5	−15.0	1.40	33.1	96.4	21.6
REF-20%	3	32.7	88.5	12.7	282	−16.9	−14.2	2.33	27.5	93.9	15.2

UPy-20% in the same range ($G' = \sim$500 MPa, Table 1), while the G'-value of REF-20% is significantly reduced ($G' = \sim$300 MPa). Overall, a clear trend regarding reactivity and shrinkage behavior is visible with increasing amounts of the monomers UPy and REF in MAM (Figure S1, Table S2-3). Adding UPy in MAM increases the reactivity compared to the addition of the REF compound in MAM and MAM itself. Furthermore, adding both monomers UPy and REF in different amounts to MAM lowers the shrinkage behavior compared to pure MAM.

2.3 | Evaluation of polymer properties

2.3.1 | Dynamic mechanical thermal analysis

The thermomechanical behavior of the photocured samples (pMAM, pUPy-20%, and pREF-20%) was evaluated via dynamic mechanical thermal analysis (DMTA, Figure 7, Table 2). The key information obtained from this measurement is the storage modulus (G') and the glass transition temperature defined as the transition from the brittle to the rubbery state and can be determined at the maximum of the tanδ curve ($T_g^{tan\delta}$) or the deflection point of the storage modulus curve ($T_g^{G'}$).

The storage modulus at 25°C (G'_{25}) indicates the stiffness of a material at this temperature. pMAM exhibits the highest value for G'_{25}, followed by pUPy-20% indicating decreased stiffness with 20 mol% UPy content. G'_{25} of pREF-20% is further reduced, suggesting its even higher flexibility. The storage modulus at the rubbery plateau (G'_{RP}) gives information about the crosslinking density of a polymeric material. pREF-20% shows the highest G'_{RP} values due to its covalent crosslinks. The non-covalent crosslinks in pUPy-20% demonstrate its thermoreversible effect by exhibiting the lowest G'_{RP} of all three systems. At elevated temperatures, the H-bonds are dissociated creating

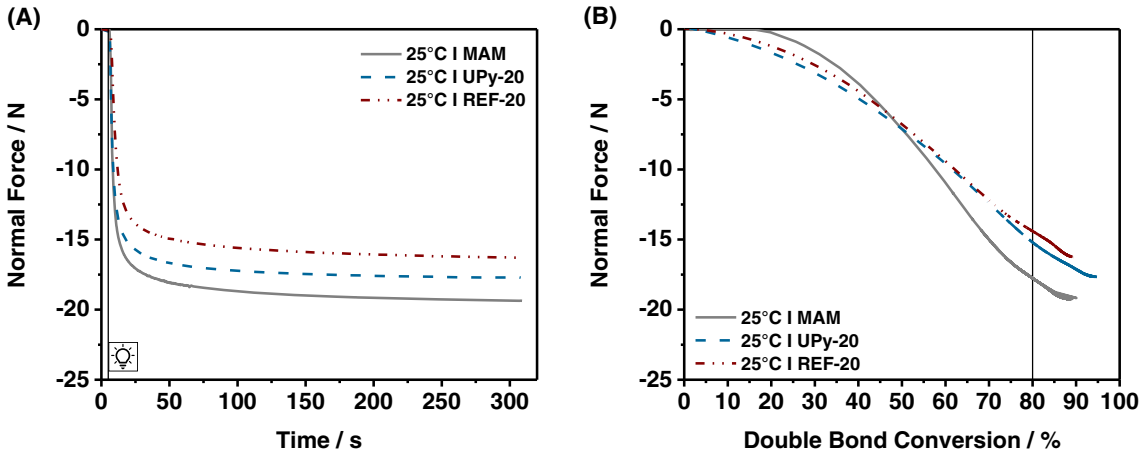

FIGURE 6 Normal force as a function of time (A) and double bond conversion (B) at 25°C of MAM, UPy-20%, and REF-20%; black line in (B) indicates $F_{N\ DBC\ 80\%}$; irradiation started after 5 s (black line in (A)).

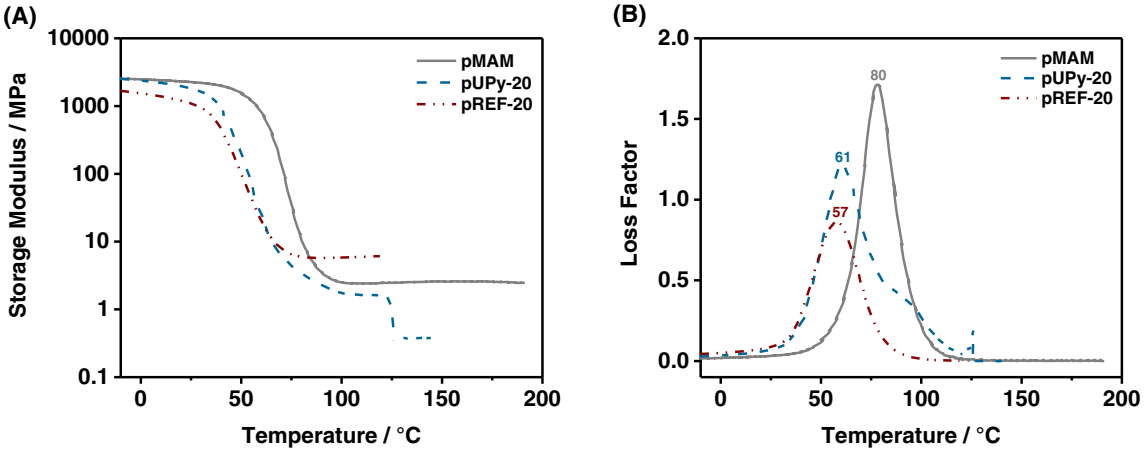

FIGURE 7 Storage modulus (G') (A) and loss factor (B) plots of pMAM, pUPy-20%, and pREF-20%.

a polymer with a linear structure. Therefore, G'_{RP} of pUPy-20% is closer to G'_{RP} of pMAM, with the value of pMAM being slightly higher due to the higher T_g of the compound. The addition of monomers UPy or REF in the photocured samples (pUPy-20% and pREF-20%) lowers the T_g by around 20°C compared to photocured MAM (pMAM). Generally, the choice of method for determining T_g depends on the application of the material, where $T_g^{tan\delta}$ is the physically defined value. However, both determination methods depict the same lowering trend in the photocured samples for the addition of UPy or REF (SI Figure S2, Table S4). This was expected since the T_g of the pure photocured compounds (pUPy-100% and pREF-100%) was more than halved compared to pMAM. The reason for these lower T_gs can be explained by the high molecular weight spacer in both compounds introducing more flexibility to the final polymer. Interestingly, the DMTA results of pUPy-20% shows a shoulder peak during the loss factor measurement with a maximum of around 80–90°C. The beginning of this second peak indicating flow of the supramolecular bonds is also visible during the DMTA measurement of pUPy-100% (Figure S2). pUPy-100% starts to melt at around 75°C due to the dissociation of H-bonds, which confirms flowing of the polymer network in pUPy-20%. Such flowing behavior is necessary for shape-reprocessing of the network.

TABLE 2 Storage modulus at 25°C (G') and glass transition temperature (T_g) measured via loss factor (tanδ), and storage modulus (G').

	G'_{25}/MPa	$T_g^{tan\delta}$/°C	$T_g^{G'}$/°C
pMAM	2320	80	58
pUPy-20%	1960	61	40
pREF-20%	1200	57	38

2.3.2 | Tensile testing

To evaluate the material's toughness and deformation behavior, tensile testing was performed investigating maximal strength (σ_M), strain at break (ε_B), stiffness, and tensile toughness (area under the stress–strain curve). The stress–strain performance of the photocured samples pMAM, pUPy-20%, and pREF-20% is presented in Figure 8A (for tensile tests of all other materials see Figure S3, Table S5). Trends of this performance can already be predicted with the results from the reactivity and thermomechanical study. Herein, early gel points with low conversions, and high glass transition temperatures often indicate brittle behavior. This could be confirmed for pMAM and pUPy-20% with ε_B as low as 2.5% and low tensile toughness of around 0.6–0.7 MJ m^{-3}. Furthermore, the σ_M values of around 40 MPa are equal to the σ values at break, which is characteristic for brittle materials. Therefore, pUPy-20% and pMAM need to be characterized as brittle, demonstrating the limited influence of UPy on the mechanical properties. On the contrary, REF exhibits increased ε_B (∼ 15%) and therefore tensile toughness is also significantly improved (4.5 MJ m^{-3}). The σ_M value of pREF-20% is similar to that of pUPy-20% and pMAM but exhibits a yield point. This indicates that REF introduces more flexibility in the final polymer than UPy. These results can be confirmed by examining the stiffness of pure polymers from one of the three monomers. pMAM exhibits the highest stiffness, followed by pUPy-20%. pREF-20% exhibits the lowest stiffness, which further underlines the increased flexibility of this difunctional monomer introduces. In UPy, the same spacer unit occurs only once per monomer, while REF always contains two units. The strong dimerization of the non-covalent H-bonds of UPy should mimic this difunctional character, which is demonstrated by the slightly improved ε_B compared to

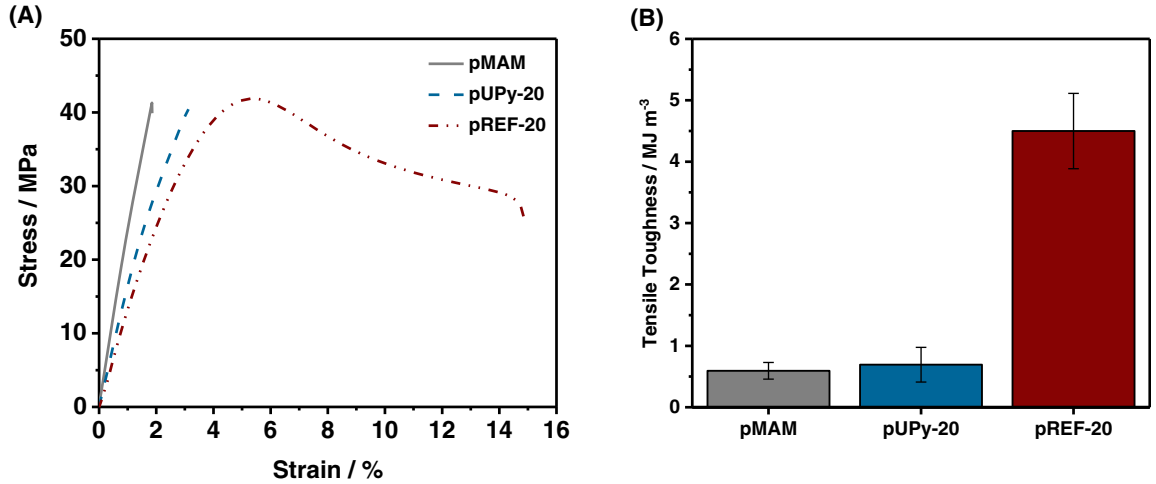

FIGURE 8 Stress–strain curves (A) and calculated tensile toughness (B) of pMAM, pUPy-20%, and pREF-20%.

MAM without a spacer (improvement: ~0.4%). Nevertheless, this dimerization of non-covalent bonds is weaker than an actual covalent bond given the possibility of dissociated or disoriented units in the photocured polymer. Therefore, increased flexibility through the spacer unit is more pronounced in pREF-20% compared to pUPy-20%. This conclusion is further supported by the order of storage moduli for these polymers at 25°C found in RT-NIR photorheology and DMTA.

2.3.3 | Investigation of dynamic behavior via stress relaxation and frequency sweep measurements

The dynamic behavior of pUPy-20% compared to pMAM and pREF-20% was characterized via stress relaxation studies. The measurement was performed with a 3-point bending test for 10 h in air at 25 and 90°C to demonstrate the thermoreversible influence of the quadruple hydrogen interactions in the polymeric system on the mechanical resilience towards a statically applied force. Stress relaxation (in %) was evaluated by comparing the stress values at each measurement point with the starting stress values. To determine the maximal stress relaxation, linear plots were most feasible but further logarithmic plots are presented in the SI (Figure S5).

At 25°C, the maximal stress relaxation of pMAM is around 51% (Figure 9, Figure S5, Table S6), followed by pREF-20% with around 74%. pUPy-20% shows a slightly higher increase to 88%. The similar relaxation of pUPy-20% and pREF-20% can be explained by the presence of H-bonding in pUPy, mimicking the difunctional character at 25°C.

At 90°C, pUPy-20% relaxes completely after around 0.5 h (26 min) due to the dissociation of H-bonds which corresponds to fewer crosslinks in the polymer network. At this point, pMAM exhibits a reduced relaxation of 41%, while pREF-20% undergoes an even lower relaxation of around 23%. The final relaxation of both polymers could be determined at around 97% for pMAM and 30% for the covalently crosslinked pREF-20%. The high final relaxation of pMAM is a result of its linear polymer structure. Since pUPy-20% also effectively has a linear character at 90°C, pUPy-20% and pMAM exhibit a similar relaxation behavior. Consequently, these results demonstrate the temperature-dependent dynamic behavior of pUPy-20% and its successful implementation in a matrix formulation to obtain a polymer network with reversible character.

The dynamic behavior of pUPy-20% was further demonstrated via frequency sweep measurements. Preliminary experiments showed that these dynamic effects are best visible at 80°C and therefore master curves of pUPy-20%

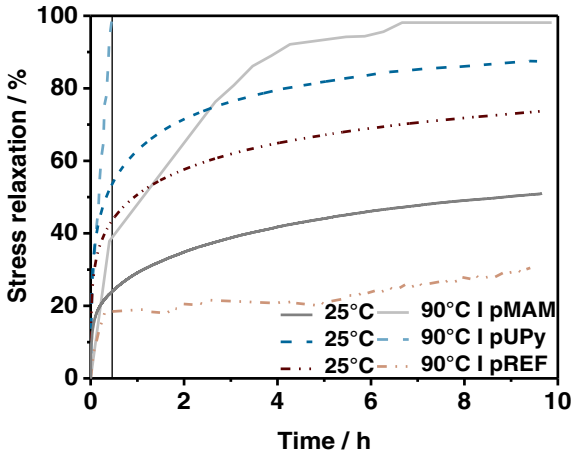

FIGURE 9 Stress relaxation plots over 10 h at 25°C and 90°C of pMAM, pUPy-20%, and pREF-20%; black line at 0.5 h (26 min) indicates the complete relaxation of pUPy-20% at 90°C.

and pREF-20% were created at this temperature. The matrix system pMAM could not be measured due to extreme brittleness of the polymerized samples leading to cracks during the measurements.

The master curve of pUPy-20% exhibits crossovers of G' and G'' at angular frequencies of around 0.25 rad s^{-1} and 1.75 rad s^{-1}, respectively, which demonstrates the dominant viscose part of pUPy at this temperature (Figure 10A and Figure S6A). On the contrary, the master curve of pREF-20% shows that the curve progression of G' is always above the one of G'' in the entire frequency range covered (Figure 10B and Figure S6B). This can be seen as dominance of elastic behavior in the material due to the lack of supramolecular interactions. At this point it should be mentioned that the depicted dynamic effect is not as pronounced as in examples utilizing only non-covalent crosslinks[45] due to the higher crosslinking density of the hybrid bonding polymers (pUPy-20% and pREF-20%).

2.3.4 | Reprocessability

The reprocessing ability of pMAM, pUPy-20%, and pREF-20% was investigated via hot pressing. Test specimens (350 ± 3 mg per sample) were cut, manually reattached, and thermally reprocessed on the hot press metal plate. Herein, the pressure between the hot press plates was varied according to Table 3, whereas the temperature was fixed at 120°C to ensure complete dissociation of the reversible H-bonding.

The measurement period ended with a cooling phase of 10 min to reach 25°C and ensure reformation of H-bonding. All three specimens were reprocessed at the

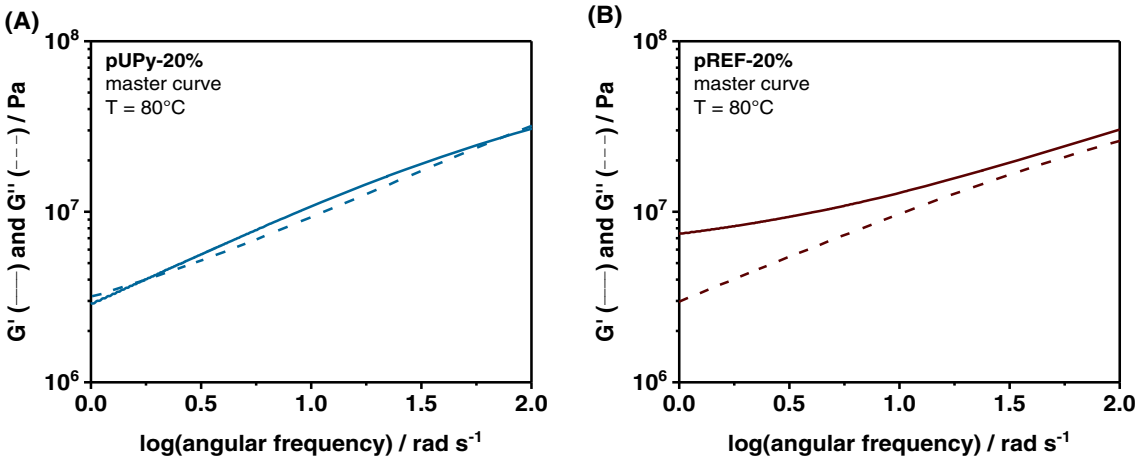

FIGURE 10 Zoomed master curves depicting frequency sweep measurements of pUPy-20% (A) and pREF-20% (B) at 80°C; master curves presented in SI Figure S6.

TABLE 3 Hot press program used for the reprocessing process.

Step	p/bar	t/min	T/°C
1	2	5	120
2	5	5	120
3	10	2	120
4	2	10	25

same time to guarantee constant conditions, cooling rates, and constant layer thickness (∼ 0.4 mm). Afterwards, the reprocessed samples were characterized via light microscopy. Herein, this transition between the pressed area (Figure 11, green, 1), the transition area (Figure 11, orange, 2), and the reprocessed area (Figure 11, blue, 3) were analyzed and approximated with an oval shape corresponding with the reprocessed shape of the sample. The reprocessing factor was calculated by comparing the reprocessed area with the total area of the sample. Since pREF-20% exhibits no reprocessing, the area in the middle of the sample and on the outer border show the same structure. Therefore, no reprocessing factor could be calculated, which is expected for a permanently crosslinked polymer. In contrast, the reprocessed pUPy-20% specimens exhibit a reprocessing factor of around 0.58 (Table 4), while pMAM shows a reprocessing factor of around 0.32. The reprocessing factor of pMAM is caused by the mainly linear structure of the final polymer, which allows melting and renewed chain entanglement to a certain degree. The small amount of crosslinker, which is present in all three polymers (pMAM, pUPy-20%, and pREF-20%), does not interfere with the H-bonds as already proven previously.[39,43] Consequently, introducing the UPy monomer (20 mol%) in MAM significantly improves the reprocessing factor, highlighting its beneficial dynamic effect.

2.4 | Hot Lithography printing process

2.4.1 | Viscosity and storage stability

One of the main benefits of Hot Lithography is the ability to process high viscous resins with high precision and resolution at temperatures up to 120°C, while commercially available additive manufacturing systems are usually limited to resins with viscosities below 1 Pa · s. Herein, the viscosity of all formulations in this temperature range was investigated to evaluate the ideal printing temperature (Figure 12A). Sufficiently low viscosity of UPy-20 was reached at 50°C.

As demonstrated in Figure 12A, adding the monomers UPy and REF to MAM increases viscosity significantly (25°C; UPy-20%: 2.7 Pa . s, REF-20%: 16.9 Pa . s, and MAM: 0.8 Pa . s, Table S7, Figure S7) due to the higher molecular weight of these monomers (25°C; UPy-100%: 4.0 Pa . s, REF-100%: 34.2 Pa . s). At 50°C, all formulations exhibit viscosities below 1.5 Pa . s, which enables easy processing via a Hot Lithography system. Therefore, 50°C was chosen as ideal printing temperature and used for further investigations.

Furthermore, formulations processed via an additive manufacturing process must exhibit sufficient storage stability at printing temperature to ensure a successful printing job. Therefore, storage stability tests were performed over five days. All three formulations were stored at printing temperature (50°C) and their viscosity was measured every 24 h at 50°C (Figure 12B). The viscosity of UPy-20%, REF-20%, and MAM (Figure 12B, Table S8) showed no significant increase over five days. Therefore, it can be concluded that all formulations exhibit sufficient stability at printing temperature to enable a purely light-driven printing process.

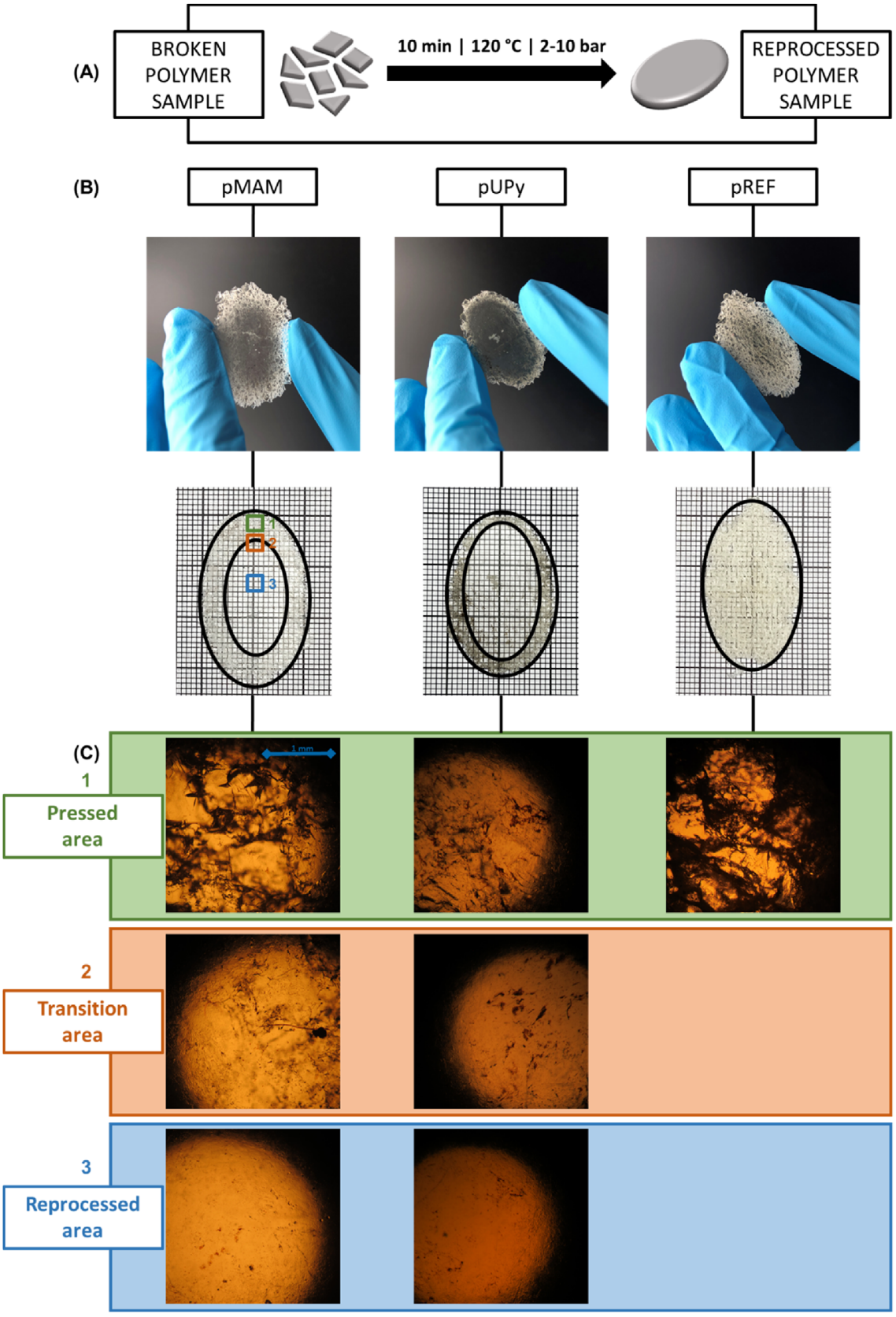

FIGURE 11 Reprocessing experiment: (A) schematic representation of the reprocessing experiment via a hot press; (B) pictures of the reprocessed samples and approximation with an oval shape of pMAM (left), pUPy-20% (middle), pREF-20% (right); (C) light microscopy pictures of pressed area (1, green), transition area (2, orange),and reprocessed area (3, blue) of pMAM (left), pUPy-20% (middle), pREF-20% (right), colored squares with numbers in (B) indicates the different areas in (C).

2.4.2 | Thermogravimetric analysis

Materials used in a Hot Lithography process also require thermal stability and low volatility at printing temperature (50°C), which can be observed via thermogravimetric analysis (TGA) using two different measurement setups. To evaluate thermal stability of the formulation, the mass loss during a temperature sweep (25 - 400°C) was recorded and evaluated. MAM, UPy-20%, and REF-20% demonstrated excellent thermal stability with mass losses of 5 wt% only at temperatures above 240°C (Table S9). Subsequently, evaporation of the formulation at a constant temperature of 50°C was investigated, mimicking the printing temperature, and determining the final mass loss after 2 h. In this study, MAM, UPy-20%, and REF-20% exhibit a mass loss below 0.2 wt% during this time interval highlighting the excellent thermal behavior of all monomeric systems (Figure S8, Table S9). Consequently, all components (UPy, REF and MAM) are suitable for Hot Lithography.

2.4.3 | Hot Lithography printing process

Commercially available lithography-based additive manufacturing systems are usually limited to low-viscous resins (typically <1 Pa . s) to obtain high precision prinited parts. Hot Lithography uses a heated bottom-up stereolithography setup, which reaches temperatures up to 120°C and can process resins up to 20 Pa . s within the same precision level. Therefore, 20 mol% UPy in MAM (Figure 13A) was processed in bulk with a DLP Hot Lithography system at 50°C using UV-light (375 nm). SEM pictures (Figure 13B) visualize the successful structuring of a defined 3D-part achieving a layer thickness of 137 µm. The high resolution of these printed layers, high accuracy in layer thickness, and the lack of light-induced or diffusional over-polymerization highlight the excellent suitability of the formulation for Hot Lithography. Additionally, the 3D-printed pyramid containing 20 mol% of UPy was reprocessed with a hot press (Figure 13A) using the same method described in the previous chapter to further promote the dynamic monomer UPy for 3D-printing applications.

TABLE 4 Reprocessing factor of pMAM, pUPy-20%, and pREF-20%.

Compound	Reprocessing factor
pMAM	0.32
pUPy-20%	0.58
pREF-20%	0

3 | CONCLUSION

The dynamic monomer UPy has successfully been implemented in a classical methacrylic matrix to obtain thermoreversible effects in a slightly crosslinked polymeric network. It could be demonstrated that UPy improves the reactivity and shrinkage behavior compared to a pure methacrylic matrix (MAM) and a similar difunctional reference compound (REF). This difunctional REF was chosen for comparison to mimic the effect of H-bonds below 80°C with covalent bonds in the polymer network. Furthermore, the mechanical properties of UPy in MAM are similar to pure MAM, whereas the glass transition temperature is reduced due to the higher molecular weight and the long spacer unit of UPy. REF further introduces flexibility in MAM, which becomes evident in the decreased glass transition temperature and mechanical behavior. Furthermore, introducing UPy in MAM leads

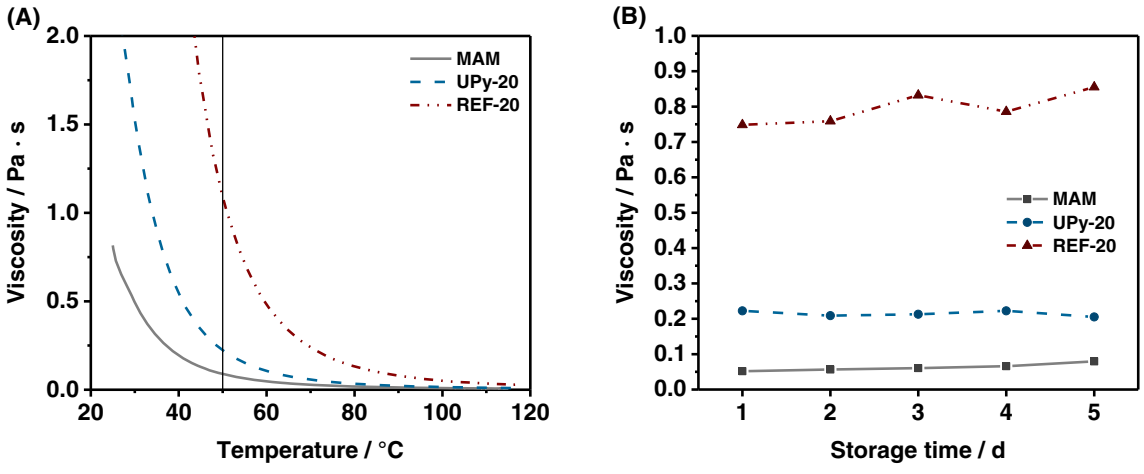

FIGURE 12 Viscosity and storage stability measurements of MAM, UPy-20%, and REF-20%: (A) viscosity during a temperature sweep experiment (25–120°C), and (B) viscosity at 50°C for formulations stored at 50°C for up to 5 days.

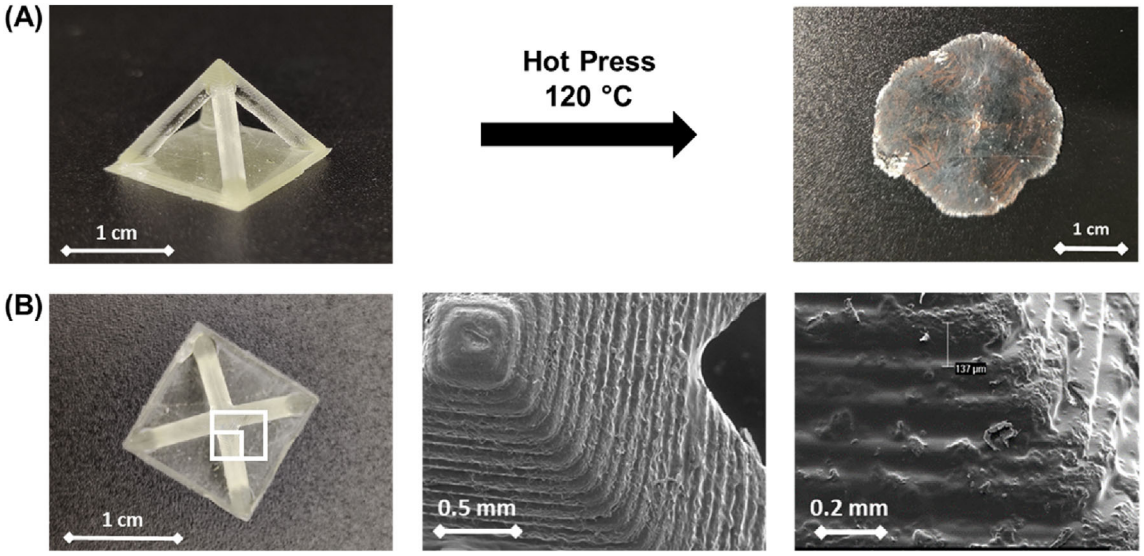

FIGURE 13 Images before and after reprocessing (A) and SEM images (B) of the 3D printed parts (20 mol% UPy in MAM).

to dynamic benefits in the polymer network, demonstrating improved stress relaxation and reprocessability. It could be shown that UPy-20% exhibits stress relaxation behavior similar to analogous materials with covalent bonds substituting the H-bonds (REF-20%) at 25°C. At elevated temperatures (90°C), however, the dissociation of the H-bonds causes similarities of the material to an analogous non-crosslinked material (MAM). These results prove the temperature-depended dynamic behavior of UPy and demonstrate the simple implementation of a reversible character in a polymer matrix.

Moreover, UPy-20% also significantly improves the temperature-triggered reprocessability evaluated via the reprocessing factor compared to the monofunctional MAM system. As expected, the difunctional REF-20% system exhibits no reprocessing potential due to its crosslinked polymer network structure. Additionally, it could be demonstrated that all formulations are suitable for 3D-printing, providing sufficiently high thermal stability and low volatility. Finally, 20 mol% UPy in MAM was processed in bulk via a Hot Lithography at 50°C yielding well-defined complex 3D-structures. These 3D-printed parts showed a high resolution and precision as well as a lack of over-polymerization highlighting the versatile benefits of the monomer UPy.

4 | MATERIALS AND METHODS

2-Amino-4-hydroxy-6-methylpyrimidine (abcr), triethylamine (Et_3N, Sigma-Aldrich), 1,1′-carbonyl-diimidazole (CDI, abcr, recrystallized in THF before usage), *p*-methoxyphenol (MEHQ, Sigma-Aldrich), phenothiazine (Sigma-Aldrich), methacrylic anhydride (abcr, distilled before usage), and 4,4′-methylenedianiline (MDA, ACROS) were purchased from the respective companies. The starting chemical amine-terminated oligo(propylene glycol) (OPG, MW: 400 g mol^{-1}) commercially available as Baxxodur® EC 302 was kindly provided by BASF. All reagents and monomers were used without any further purification, unless mentioned otherwise. Commercial grade dichloromethane (CH_2Cl_2, Donau Chemie) and tetrahydrofuran (THF, Donau Chemie) were dried using a PureSolv system (Inert, Amesbury, MA).

Column chromatography was performed on a Büchi Sepacore Flash System (Büchi pump module C-605, Büchi control unit C-620, Büchi UV-Photometer C-635, Büchi fraction collector C-660), using glass columns packed with silica gel 60 (Merck, 0.040–0.063 mm) or aluminum oxide 90 neutral (Carl Roth). NMR-spectra were recorded on a Bruker Avance DRX-400 FT-NMR spectrometer at 400 MHz for ^{1}H- and at 100 MHz for ^{13}C-spectra. The signals are reported with their chemical shifts in ppm and fine structure (s = singlet, d = doublet, t = triplet, q = quartet, qn = quintet, sep = septet, m = multiplet). The chemical shifts were referenced by using the respective NMR-solvent [^{1}H: $CDCl_3$ (7.26 ppm), ^{13}C: $CDCl_3$ (77.16 ppm)] as internal reference. HR-MS analysis was performed for all synthesized monomers dissolved in HPLC-grade acetonitrile (10 µM).

4.1 | Synthesis of UPy- and REF-compound

4.1.1 | Synthesis of N-(6-methyl-4-oxo-1H-pyrimidin-2-yl)-1H-imidazole-1-carboxamide (3)

The synthesis of (3) was performed according to a procedure published by Wong et al.[41] A mixture of 2-amino-

4-hydroxy-6-methylpyrimidine (1) (1.0 equ., 8.56 g, 68.4 mmol) and 1,1′-carbonyl-diimidazole (2) (1.3 equ., 14.43 g, 89.0 mmol) in dry THF was heated to reflux (85°C) for 12 h under argon atmosphere. Afterwards, the suspension was cooled to 25°C and filtered. The white precipitate was washed with cold acetone (2 × 100 ml) and dried under vacuum to yield (3) as a white solid (13.86 g, 92.6%). (3) was characterized via ATR-IR spectroscopy and it was used in the subsequent step without further purification. R_f 0.63 (EE:MeOH 1:1).

IR (ATR): ν (cm^{-1}): 3174, 3068, 2637 (bs), 1699, 1641, 1598, 1508, 1470, 1371, 1334, 1317, 1275, 1232, 1223, 1190, 1168, 1089, 1063, 1025, 982, 911, 852, 799, 777, 759, 647, 605, 575, 561.

4.1.2 | Synthesis of UPy-OPG-amine (5)

The synthesis of (5) was performed according to a modified procedure published by Heinzmann et al.[37] (3) (1.0 equ., 10.00 g, 45.6 mmol) was dispersed in an amine-terminated oligo(propylene glycol) (4) (5.0 equ., 104.20 g, 228.1 mmol) under argon atmosphere and heated up to 45°C overnight. The clear liquid was poured into cold hexane to precipitate a yellow, oily liquid, which was collected and diluted with chloroform. This organic phase was then washed with brine and deionized water and afterwards dried with Na_2SO_4. After filtration, the solvent was removed under reduced pressure. The crude product was purified by flash column chromatography (EE:MeOH, gradient MeOH 5 to 50%) and yielded (5) as a clear, slightly yellow oil (20.44 g, 73.7%). R_f 0.63 (EE:MeOH 1:1).

^{1}H NMR (400 MHz, $CDCl_3$) δ (ppm): 11.85 (s, 1H), 9.98 (s, 1H), 5.78 (s, 1H), 4.00 (s, 1H), 3.74–2.97 (m, 22H), 2.17 (d, J = 13.4 Hz, 3H), 1.31–1.19 (m, 3H), 1.19–0.91 (m, 20H).

^{13}C NMR (APT) (101 MHz, $CDCl_3$) δ (ppm): 171.12, 156.00, 154.77, 154.70, 75.47, 75.36, 75.13, 75.02, 73.27, 73.01, 72.97, 72.90, 60.37, 50.09, 47.00, 46.52, 46.50, 45.91, 21.03, 17.36, 17.29, 17.25, 17.17, 16.93, 14.19.

4.1.3 | Synthesis of UPy-OPG-methacrylamide (UPy, (7))

The synthesis of UPy (7) was performed according to a modified procedure published by Heinzmann et al.[37] (5) (1.0 equ., 6.88 g, 11.2 mmol) was diluted with dry CH_2Cl_2 under argon atmosphere and cooled down to 0°C with a NaCl/ice-bath. Then, Et_3N (2.5 equ., 2.83 g, 28.0 mmol) diluted with dry CH_2Cl_2 was added dropwise and the reaction mixture, which was then stirred for 1 h. Afterwards, freshly distilled methacrylic anhydride (6) (2.3 equ., 3.97 g, 25.7 mmol) diluted with dry CH_2Cl_2 was added dropwise and the reaction mixture was further stirred at room temperature for 12 h. The organic phase was washed with brine, dried over Na_2SO_4, filtered, and the solvent was removed under reduced pressure. The crude product was purified by flash column chromatography (EE:MeOH, gradient MeOH 0 to 5%) to yield UPy (7) as clear, slightly yellow oil (3.50 g, 46.3%). The pure product was stabilized with 400 ppm MEHQ and 400 ppm phenothiazine as inhibitor. R_f 0.32 (EE:MeOH 9:1).

Purity (HPLC): t_R = 15.1788 min (80% methanol/20% water, v/v, detection at 270 nm).

^{1}H NMR (400 MHz, $CDCl_3$) δ (ppm): 13.08 (s, 1H), 11.84 (s, 1H), 9.98 (s, 1H), 6.51–6.00 (m, 1H), 5.78 (t, 1H), 5.78 (s, 1H), 5.27 (s, 1H), 4.31–3.06 (m, 23H), 2.19 (s, 3H), 1.93 (t, 3H), 1.15 (m, 23H).

^{13}C NMR (101 MHz, $CDCl_3$) δ (ppm): 172.87, 167.91, 156.29, 154.79, 148.12, 140.45, 119.21, 106.82, 76.08, 75.62, 75.28, 75.08, 73.47, 72.99, 72.64, 72.16, 72.01, 46.47, 46.19, 45.61, 45.41, 21.13, 19.01, 18.83, 18.74, 17.79, 17.49, 17.39, 17.36, 17.10, 14.29.

4.1.4 | Synthesis of N-(p-{[p-(1H-Imidazol-1-ylcarbonylamino)phenyl]methyl}phenyl)-1H-imidazole-1-carbox-amide (9)

The synthesis of (9) was performed according to a modified procedure published by Wong et al.[41] A mixture of 4,4′-methylenedianiline (8) (1.0 equ., 15.39 g, 77.6 mmol) and 1,1′-carbonyl-diimidazole (2) (1.3 equ., 30.21 g, 186.3 mmol) in dry THF was heated to reflux (85°C) for 12 h under argon atmosphere. Afterwards, the suspension was cooled to 25°C and filtered. The yellow precipitate was washed with cold THF and dried under vacuum to yield (9) as a slightly yellowish solid (21.12 g, 70.4%).^{1}H NMR (400 MHz, DMSO) δ (ppm): 10.26 (s, 2H), 8.39 (s, 2H), 7.82 (t, 2H), 7.57–7.49 (m, 4H), 7.27 (m, 4H), 7.12–7.08 (m, 2H), 3.94 (s, 2H).

^{13}C NMR (APT) (101 MHz, DMSO) δ (ppm): 146.87, 137.62, 135.41, 129.63, 129.05, 128.97, 121.18, 117.05.

4.1.5 | Synthesis of MDA-bis(OPG-amine) (10)

The synthesis of (10) was performed according to a modified procedure published by Heinzmann et al.[37] (9) (1.0 equ., 20.00 g, 51.8 mmol) was dispersed in an amine-terminated oligo(propylene glycol) (4) (5.0 equ., 118.22 g, 258.8 mmol) under argon atmosphere and heated up to 45°C overnight. The clear liquid was poured into cold hexane to precipitate a yellow, oily liquid. The oily liquid was collected and diluted with CH_2Cl_2, which was

washed with brine. Afterwards, the organic phase was dried with Na_2SO_4, filtered, and the solvent was removed under reduced pressure to yield (10) as an orange oil (47.99 g, 79.65%). R_f 0.41 (EE:MeOH 95:5).

^{1}H NMR (400 MHz, DMSO) δ (ppm): 8.39 (d, 2H), 7.27 (d, 4H), 7.04–6.97 (m, 4H), 6.00–5.90 (m, 2H), 3.86–3.72 (m, 4H), 3.58–3.23 (m, 42H), 3.13 (m, 2H), 1.14–0.99 (m, 41H), 0.94–0.89 (m, 6H).

^{13}C NMR (APT) (101 MHz, DMSO) δ (ppm): 154.65, 138.39, 134.11, 128.71, 117.62, 75.58, 74.56, 72.19, 46.22, 44.94, 19.84, 17.07.

4.1.6 | Synthesis of MDA-bis(OPG-methacrylamide) (REF, (11))

The synthesis of REF (11) was performed according to a modified procedure published by Heinzmann et al.[37] (10) (1.0 equ., 40.00 g, 34.4 mmol) was diluted with dry CH_2Cl_2 under argon atmosphere and cooled to 0°C with a NaCl/ice-bath. Then, Et_3N (5.0 equ., 17.39 g, 171.8 mmol) diluted with dry CH_2Cl_2 was added dropwise and the reaction mixture was stirred for 1 h. Afterwards, freshly distilled methacrylic anhydride (5 equ., 26.49 g, 171.8 mmol) diluted with dry CH_2Cl_2 was added dropwise and the reaction mixture was further stirred at room temperature for 5 d. The organic phase was washed with brine, dried over Na_2SO_4, filtered, and the solvent was removed under reduced pressure. The crude product was purified by flash column chromatography (EE:MeOH, gradient MeOH 0 to 5%) to yield REF (11) as clear, slightly yellow oil (8.23, 18.4%). The pure product was stabilized with 400 ppm MEHQ and 400 ppm phenothiazine as inhibitor. $R_f = 0.76$ (EE:MeOH 8:2).

Purity (HPLC): $t_R = 17.2183$ min (80% methanol/20% water, v/v, detection at 270 nm).

^{1}H NMR (400 MHz, DMSO) δ (ppm): 8.34 (d, 2H), 7.54 (d, 2H), 7.30–7.22 (m, 4H), 7.05–6.98 (m, 4H), 5.99–5.89 (m, 2H), 5.65–5.60 (m, 2H), 5.29 (m, 2H), 3.84–3.70 (m, 4H), 3.59–3.21 (m, 38H), 1.84 (t, 6H), 1.17 (t, 6H), 1.11–0.94 (m, 42H).

^{13}C NMR (APT) (101 MHz, DMSO) δ (ppm): 167.02, 154.63, 140.15, 138.39, 134.13, 128.72, 118.66, 117.64, 74.66, 74.59, 74.36, 74.25, 72.39, 72.17, 72.02, 71.57, 71.52, 71.32, 59.73, 44.96, 44.79, 44.75, 44.52, 20.72, 18.66, 18.07, 17.28, 17.23, 17.11, 17.06, 14.06.

4.2 | RT-NIR photorheology

Real time near infrared (RT-NIR) photorheology measurements were performed on an Anton Paar MCR 302 WESP rheometer, which is equipped with a P-PTD 200/GL Peltier glass plate and a PP25 measuring system with a Bruker Vertex 80 Fourier-Transform Infrared (FTIR) spectrometer to measure the conversion over time. Further information about the measurement set-up and procedure can be found in literature.[44] For each photorheological measurement, 150 µl formulation and a constant gap size of 200 µm was used. The temperature was controlled by an Anton Paar H-PTD 200 heating hood. The formulations were sheared with a strain of 1% and a frequency of 1 Hz. To initiate the photopolymerization reaction, UV-light was powered from the optical window underneath the formulation. An Exfo OmniCure™ 2000 device with a broadband Hg-lamp was used as external UV-source. The following irradiation conditions were used: 300 s, 400–500 nm, ∼ 30 mW cm^{-2} on the surface of the sample, which was measured with an Ocean Optics USB 2000+ spectrometer. Additionally, a polyethene tape (TESA 4668 MDPE) was applied on the optical window of the lower rheometer plate to ensure smooth removal of the photopolymerized specimens. The rheometer device records the storage modulus (G') and loss modulus (G'') according to the following time interval pattern: one measurement point per second before initiation, one measurement point per 0.2 s during the first 60 s, one measurement point per second until the irradiation period ends (4 min). The double bond conversion (DBC) of the (meth)acrylic end groups was obtained by recording a set of single spectra (time interval ∼ 0.26 s) with the OPUS 7.0 software and integrating the DB-signals at a wavelength of around 6100–6300 cm^{-1}. The DBC was then determined via the ratio of the peak area at the start and at the end of the measurement. All measurements were performed in triplicates.[44]

4.3 | Dynamic mechanical thermal analysis

The dynamic mechanic thermal analysis (DMTA) measurements were conducted with an Anton Paar MCR 302 with a CTD 450 oven and an SRF 12 measuring system. All specimens were tested in torsion mode with a frequency of 1 Hz, a strain of 0.1%, and a temperature range from −100 to 200°C using a heating rate of 2°C min^{-1}. The software Rheoplus/32 V3.40 from Anton Paar was used to record the storage modulus (G') and loss factor (tanδ) of the polymer samples. The glass transition temperature (T_g) was obtained from the maximum of the loss factor ($T_g^{\tan\delta}$) and the turning point of the storage modulus plot ($T_g^{G'}$).

4.4 | Tensile testing

Tensile tests were performed on a Zwick Z050, which was equipped with a 1 kN load cell. A crosshead speed of 5 mm min^{-1} was used to strain the specimens of type 5B

according to ISO 527-2. A stress–strain plot was recorded during this measurement. Five specimens were tested for each formulation with satisfactory reproducibility.

4.5 | Stress relaxation

Stress relaxation measurements were performed in a 3-point bending setup under air on a RSA G2 Solids Analyzer test apparatus (TA Instruments, New Castle, USA), using a strain of 1%. The measurements were conducted at 25 and 90°C over a time span of 10 h. The stress behavior (in MPa) was recorded over time (in s) during this measurement setup. The stress relaxation (in %) could then be calculated by normalizing to the starting values (average of 10 values). The data points evaluated at 90°C needed to be smoothed via an adjacent average using every 100th data point, since the measurements were performed over the glass transition temperature of all compounds were located close to the measurement limit of the measurement set up. Each formulation was measured once due to the good reproducibility and the duration of the measurement.

4.6 | Frequency sweep measurements

The frequency sweep measurements were conducted with an Anton Paar MCR 302 rheometer with a CTD 450 oven and an SRF 12 measuring system. All specimens were tested in torsion mode with a shear strain of 1% and an angular frequency range from 0.0001 to 100 rad s^{-1} using a logaritimic ramp at a temperature of 70 and 80°C. Before measuring, the sample was conditioned at the corresponding temperature for 30 min using with a shear strain of 1% and an angular frequency of 1 rad s^{-1}. The software Rheoplus/32 V3.40 from Anton Paar was used to record the storage modulus (G') and loss modulus (G'') of the polymer samples. To extend the frequency range to somewhat higher values master curves were constructed by measuring the same sample at different temperatures (70 and 80°C). Both temperatures are above T_g and the materials should be similar from a thermo-rheologic point of view in that case and horizontal shifting the 70°C curve for merging with the reference curve at 80°C according to the temperature–time equivalency law.

4.7 | Reprocessability

Reprocessability tests were performed with a Collin P 200 P heating press. Broken testing specimens (around 350 mg per sample) were reattached on the metal plate using the following heating and pressure program (Table 3). After a cooling period of 10 min to ensure the reformation of H-bonding without any outer influence, reprocessed samples were analyzed via optical light microscopy. The pressed samples were approximated with an oval shape to evaluate the reprocessing factor. Therefore, the reprocessed area was compared with the total area of the sample. The transition area was determined via light microscopy and it is defined as border between the reprocessed and the processed area. For comparison, all three areas (reprocessed, transition, and pressed) were approximated with an oval shape, which corresponds to the overall shape of all samples (pMAM, pUPy-20%, and pREF-20%) after treatment. All three specimens were tested once and were reprocessed at the same time to guarantee constant conditions and constant layer thickness ($\sim$ 0.4 mm).

4.8 | Optical light microscopy

The reprocessed samples were analyzed via optical light microscopy to investigate the ratio of reprocessed area compared to pressed area. This measurement was performed on a Zeiss Axio Scope.A1.

4.9 | Thermogravimetric analysis and volatility study

The thermogravimetric analysis (TGA) was performed on a Netzsch Jupiter STA 449 F1 thermal analysis instrument with autosampler, which combines TGA and DSC experiments. All formulations were investigated regarding their volatility and thermal stability. One set of measurements (study 1) was performed with a temperature ramp from 25 to 400°C under N_2 atmosphere (10 K min^{-1}), and the second set (study 2) was conducted isothermally under N_2 atmosphere at 50°C (2 h), which corresponds to the printing temperature. All samples were accurately weighed into aluminum DSC pans (12 $\pm$ 2 mg) and measured at a constant gas flow rate (40 ml min^{-1}). During this measurement, the mass loss and DSC signal were recorded over time and all samples were measured once.

4.10 | Viscosity measurements

The viscosity of the neat monomers as well as freshly prepared monomeric formulations were performed with a rheological measurement system. The rheology measurements

were carried out on an Anton Paar MCR 300 apparatus equipped with a Peltier temperature control unit and a CP-25-1 measuring system. The measurements were performed with 80 µl of each sample, using a gap distance of 50 µm between cone and bottom plate. First, the dynamic viscosity was recorded over time during the first 50 s, while the sheer rate was gradually increased from 1 to 100 s^{-1}. Afterwards, the viscosity was recorded from 25 to 120°C over the course of 200 s (heating rate: ~ 2°C s^{-1}), using a constant shear rate of 100 s^{-1}. Each measurement was performed in triplicates to guarantee reproducibility.

For the storage stability tests, the same rheological device was used. Herein, the viscosity of the formulations was measured at the printing temperature of 50°C (5 min acclimatization time before measurement) with a CP-25-1 measuring system and a gab distance of 50 µm. Measurements were conducted in rotation mode with a constant shear rate of 100 s^{-1}. The same formulation, which was stored at 50°C, was measured once per day over a time span of 5 days and the viscosity change was recorded over time.

4.11 | Hot Lithography additive manufacturing system

The printing process was performed on a BP5 (Blue Printer 5 of TU Wien) with a digital light processing (DLP) system using a transparent, rotatable, and heated material vat. The liquid resin was dispensed on this material vat, showing a temperature of around 50°C during the printing process. The three-dimensional matrix was created with a digital mirror device (DMD) projected UV-light (375 nm). The building process was performed in a layer-by-layer and bottom-up mode. The fresh resin was coated with a plate on the material vat after solidifying each layer. The coating process combined a rotatable vat and a coating knife to ensure equal good resin circulation. The Luxbeam 4600 of Visitech Engineering GmbH (Wetzlar, Germany) was used as light engine. The three-dimensional model was created out of a Common Layer Interface (CLI) file, which was transformed in 500 png files, to provide the light exposure information of each image.

4.12 | Scanning electron microscope

The 3D printed parts were characterized via a scanning electron microscope (SEM) to determine the layer thickness and possible void formation. The morphology was imaged with a Phillips XL-30 after sputtering with a thin gold layer.

4.13 | Reprocessing via hot pressing

Reprocessability tests were performed with a Collin P 200 P heating press. The 3D printed test specimen (pyramid) was placed on the metal plate of the hot press using the following heating and pressure program (Table 3). At the end, a cooling period of 10 min was programmed to ensure the reformation of H-bonding without any outer influence.

ACKNOWLEDGMENTS

The matrix monomer 2-(2-biphenylyloxy)ethyl methacrylate was kindly provided by the company Ivoclar Vivadent. Baxxodur® EC 302 was kindly provided by the company BASF. Special thanks to Olja Dragojevic for the experimental support. The authors acknowledge TU Wien Bibliothek for financial support through its Open Access Funding Programme.

DATA AVAILABILITY STATEMENT

The data that support the findings of this study are available on request from the corresponding author. The data are not publicly available due to privacy or ethical restrictions.

ORCID

Larissa Alena Ruppitsch https://orcid.org/0000-0003-3151-8948
Katharina Ehrmann https://orcid.org/0000-0002-0161-0527
Jürgen Stampfl https://orcid.org/0000-0002-3626-5647
Robert Liska https://orcid.org/0000-0001-7865-1936

REFERENCES

[1] S. I. Stupp, V. LeBonheur, K. Walker, L. S. Li, K. E. Huggins, M. Keser, A. Amstutz, *Science* **1997**, *276*(5311), 384.
[2] R. P. Sijbesma, F. H. Beijer, L. Brunsveld, B. J. B. Folmer, J. H. K. K. Hirschberg, R. F. M. Lange, J. K. L. Lowe, E. W. Meijer, *Science* **1997**, *278*(5343), 1601.
[3] T. D. Clemons, S. I. Stupp, *Prog. Polym. Sci.* **2020**, *111*(101), 310.
[4] T. Aida, E. W. Meijer, S. I. Stupp, *Science* **2012**, *335*(6070), 813.
[5] C. J. Kloxin, C. N. Bowman, *Chem. Soc. Rev.* **2013**, *42*(17), 7161.
[6] M. Podgórski, B. D. Fairbanks, B. E. Kirkpatrick, M. McBride, A. Martinez, A. Dobson, N. J. Bongiardina, C. N. Bowman, *Adv. Mater.* **2020**, *32*(20), 1906876.
[7] R. J. Wojtecki, M. A. Meador, S. J. Rowan, *Nature Mater.* **2011**, *10*(1), 14.
[8] X. Yan, F. Wang, B. Zheng, F. Huang, *Chem. Soc. Rev.* **2012**, *41*(18), 6042.
[9] C.-C. Cheng, F.-C. Chang, J.-K. Chen, T.-Y. Wang, D.-J. Lee, *RSC Adv.* **2015**, *5*(122), 101148.
[10] M. Burnworth, L. Tang, J. R. Kumpfer, A. J. Duncan, F. L. Beyer, G. L. Fiore, S. J. Rowan, C. Weder, *Nature* **2011**, *472*(7343), 334.

[11] J. Li, J. A. Viveros, M. H. Wrue, M. Anthamatten, *Adv. Mater.* **2007**, *19*(19), 2851.
[12] T. Ware, K. Hearon, A. Lonnecker, K. L. Wooley, D. J. Maitland, W. Voit, *Macromolecules* **2012**, *45*(2), 1062.
[13] R. Hoogenboom, *Angewandte Chemie International Edition* **2012**, *51*(48), 11942.
[14] C. Heinzmann, S. Coulibaly, A. Roulin, G. L. Fiore, C. Weder, *ACS Appl. Mater. Interfaces* **2014**, *6*(7), 4713.
[15] Hoorne-van Gemert, G. M. L.; Janssen, H. M.; Meijer, E. W.; Bosman, A. W. WO2008063057A2, May 29, **2008**.
[16] Sijbesma, R. P.; Beijer, F. H.; Brunsveld, L.; Meijer, E. W. WO9814504, April 09, **1998**.
[17] W. Niu, Y. Zhu, R. Wang, Z. Lu, X. Liu, J. Sun, *ACS Appl. Mater. Interfaces* **2020**, *12*(27), 30805.
[18] N. Zheng, Y. Xu, Q. Zhao, T. Xie, *Chem. Rev.* **2021**, *121*(3), 1716.
[19] Grimaldi, S.; Gillet, J.-P.; Hidalgo, M.; Tournilhac, F.-G.; Cordier, P.; Leibler, L. WO2008029065A2, March 13, **2008**.
[20] Leibler, L.; Montarnal, D.; Tournilhac, F.; Capelot, M. WO2012152859A1, November 15, **2012**.
[21] S. I. Stupp, T. D. Clemons, J. K. Carrow, H. Sai, L. C. Palmer, *Israel J. Chem.* **2020**, *60*(1–2), 124.
[22] Z. Zhang, L. Cheng, J. Zhao, L. Wang, K. Liu, W. Yu, X. Yan, *Angewandte Chemie Int. Ed.* **2020**, *59*(29), 12139.
[23] W. Binder, W. H. Binder, L. Bouteiller, G. Brinke, O. Ikkala, V. M. Rotello, J. Ruokolainen, S. Srivastava, H. Xu, R. Zirbs, *Hydrogen Bonded Polymers*, Springer, Berlin Heidelberg **2007**.
[24] D. P. Street, W. K. Ledford, A. A. Allison, S. Patterson, D. L. Pickel, B. S. Lokitz, J. M. Messman, S. M. Kilbey, *Macromolecules* **2019**, *52*(15), 5574.
[25] A. W. Bosman, R. P. Sijbesma, E. W. Meijer, *Mater. Today* **2004**, *7*(4), 34.
[26] C. Li, A. Iscen, H. Sai, K. Sato, N. A. Sather, S. M. Chin, Z. Álvarez, L. C. Palmer, G. C. Schatz, S. I. Stupp, *Nature Mater.* **2020**, *19*(8), 900.
[27] P. Wei, X. Yan, F. Huang, *Chem. Soc. Rev.* **2015**, *44*(3), 815.
[28] J. B. Beck, S. J. Rowan, *J. Am. Chem. Soc.* **2003**, *125*(46), 13922.
[29] S. Xiao, J. Tang, T. Beetz, X. Guo, N. Tremblay, T. Siegrist, Y. Zhu, M. Steigerwald, C. Nuckolls, *J. Am. Chem. Soc.* **2006**, *128*(33), 10700.
[30] Y. Yang, M. W. Urban, *Adv. Mater. Interfaces* **2018**, *5*(17), 1800384.
[31] F. H. Beijer, R. P. Sijbesma, H. Kooijman, A. L. Spek, E. W. Meijer, *J. Am. Chem. Soc.* **1998**, *120*(27), 6761.
[32] S. H. M. Söntjens, R. P. Sijbesma, M. H. P. van Genderen, E. W. Meijer, *J. Am. Chem. Soc.* **2000**, *122*(31), 7487.
[33] K. Yamauchi, J. R. Lizotte, T. E. Long, *Macromolecules* **2003**, *36*(4), 1083.
[34] C. L. Elkins, T. Park, M. G. McKee, T. E. Long, *J. Polym. Sci. Part A: Polym. Chem.* **2005**, *43*(19), 4618.
[35] X. Chen, P. Fei, K. A. Cavicchi, W. Yang, N. Ayres, *Colloid Polym. Sci.* **2014**, *292*(2), 477.
[36] C. Heinzmann, U. Salz, N. Moszner, G. L. Fiore, C. Weder, *ACS Appl. Mater. Interfaces* **2015**, *7*(24), 13395.
[37] C. Heinzmann, I. Lamparth, K. Rist, N. Moszner, G. L. Fiore, C. Weder, *Macromolecules* **2015**, *48*(22), 8128.
[38] K. B. Manning, N. Wyatt, L. Hughes, A. Cook, N. H. Giron, E. Martinez, C. G. Campbell, M. C. Celina, *Macromol. Mater. Eng.* **2019**, *304*(3), 1800511.
[39] M. Invernizzi, S. Turri, M. Levi, R. Suriano, *Eur. Polym. J.* **2018**, *101*, 169.
[40] M. Pfaffinger, *Laser Technik J.l* **2018**, *15*(4), 45.
[41] C.-H. Wong, H.-F. Chow, S.-K. Hui, K.-H. Sze, *Org. Lett.* **2006**, *8*(9), 1811.
[42] Y. Catel, J. Angermann, P. Fässler, U. Fischer, T. Schnur, N. Moszner, *Dental Mater.* **2021**, *37*(2), 351.
[43] J. Yan, M. Li, Z. Wang, C. Chen, C. Ma, G. Yang, *Chem. Eng. J.* **2020**, *389*(123), 468.
[44] C. Gorsche, R. Harikrishna, S. Baudis, P. Knaack, B. Husar, J. Laeuger, H. Hoffmann, R. Liska, *Anal. Chem.* **2017**, *89*(9), 4958.
[45] M. Golkaram, K. Loos, *Macromolecules* **2019**, *52*(24), 9427.

SUPPORTING INFORMATION

Additional supporting information can be found online in the Supporting Information section at the end of this article.

How to cite this article: L. A. Ruppitsch, J. Ecker, T. Koch, K. Ehrmann, J. Stampfl, R. Liska, *J. Polym. Sci.* **2023**, *61*(13), 1318. https://doi.org/10.1002/pol.20220721